Impact of discontinuous deformation upon the rate of chaotic mixing

Lachlan D. Smith,[1,2,3,*] Murray Rudman,[2] Daniel R. Lester,[4] and Guy Metcalfe[5,6,7]

[1]*Department of Chemical and Biological Engineering, Northwestern University, Evanston, Illinois 60208, USA*
[2]*Department of Mechanical and Aerospace Engineering, Monash University, Clayton, Victoria 3800, Australia*
[3]*CSIRO Mineral Resources, Clayton, Victoria 3800, Australia*
[4]*School of Engineering, RMIT University, Melbourne, Victoria 3000, Australia*
[5]*School of Mathematical Sciences, Monash University, Clayton, Victoria 3800, Australia*
[6]*CSIRO Manufacturing, Highett, Victoria 3190, Australia*
[7]*Department of Mechanical and Product Design Engineering, Swinburne University of Technology, Hawthorn, Victoria 3122, Australia*

Mixing in smoothly deforming systems is achieved by repeated stretching and folding of material, and has been widely studied. However, for the classes of materials that also admit discontinuous deformation, the theory of mixing based on the assumption of smooth deformation does not apply. Discontinuous deformation provides additional topological freedom for material transport and results in different Lagrangian coherent structures forbidden in smoothly deforming systems. We uncover the impact of discontinuous deformation on mixing rates, showing that mixing can be either enhanced or impeded depending on the local stability of the underlying smooth map.

I. INTRODUCTION

Efficient mixing is essential to many physical processes and engineering applications, from the microscale [1] to the geological and oceanic scales [2–4]. In smooth fluid flows, mixing is achieved via chaotic advection [5,6], driven by repeated stretching and folding (SF) of fluid. Sampling a periodic incompressible flow after each period results in a smooth volume-preserving map. Therefore, the dynamics of smooth flows can be studied using the theory of volume-preserving maps, which have been studied extensively.

While the majority of flows involve only smooth deformations (stretching, folding, shear, etc.), there also exist fluid flows and materials that exhibit discontinuous deformations (cutting, rearranging), termed Lagrangian discontinuities. For instance, fluid flows with valves [7,8] and granular flows [9–14] can generate discontinuous deformations, while shear-banding materials such as colloidal suspensions, plastics, polymers, and alloys [15–17] naturally produce discontinuous deformations in smooth underlying velocity fields due to localized failure. In these systems, mixing can also be generated via cutting and shuffling (CS) actions, like shuffling a deck of cards. Even though CS cannot generate chaos, it can still achieve complete mixing under appropriate conditions [14,18,19].

However, not all complete mixing is equal: For practical applications, the rate of mixing is also important, and we need to organize the different types of mixing that form the ergodic hierarchy [14]. Strong mixing, characterized by a positive Lyapunov exponent (the rate of elongation of material lines), is typical of chaotic SF systems. In contrast, CS systems have an identically zero Lyapunov exponent and are only able to achieve weak mixing characterized by much slower algebraic mixing rates. Therefore, in systems with CS and equal Lyapunov exponent, other measures are

needed to distinguish between the rates of mixing achieved. An alternative measure is the mix-norm [20], a multiscale measure for mixing that is able to quantify the rate of mixing for both SF and CS mechanisms.

While purely discontinuous deformation rarely occurs in practice, most studies on mixing in the presence of discontinuous deformation have focused on cases where only cutting and rearranging are allowed, where the mixing phenomena is couched in terms of piecewise isometries [21–26]. Few studies have considered mixing in systems with combined SF and CS actions. It has been shown that the Lagrangian coherent structures inherit characteristics of both SF and CS systems, but the nature of these structures and their governing mechanics are not well understood [8]. The presence of discontinuous deformations invalidates the Hamiltonian framework, destroys impenetrable barriers to transport, and creates pseudoperiodic points, which can be thought of as classical periodic points that are seemingly destroyed by discontinuous deformation, inheriting some of their properties. Like regular periodic points, the character of pseudoperiodic points influences the deformation dynamics in the local neighbourhood around them. Like elliptic periodic points in smooth systems, particles rotate about pseudoelliptic points; however, there are no KAM-tori that form impenetrable barriers to transport surrounding them. Instead, pseudoelliptic points are surrounded by leaky regions where particles are loosely confined. Pseudohyperbolic points play a similar role to hyperbolic periodic points, generating mixing. However, mixing is confined to the closure of the measure zero set of all images or preimages of the cutting line, termed the "web of images or preimages" of the Lagrangian discontinuity [8], or the "exceptional set" in the theory of piecewise isometries [23]. Like the chaotic sea generated by hyperbolic points, the web of preimages can have positive area, though in many cases it has measure zero. It is unknown what impact these structures have on the rate of mixing and transport. By adding a discontinuous slip deformation to a linear volume-preserving map, we show that the existence of pseudoelliptic points decreases the rate of
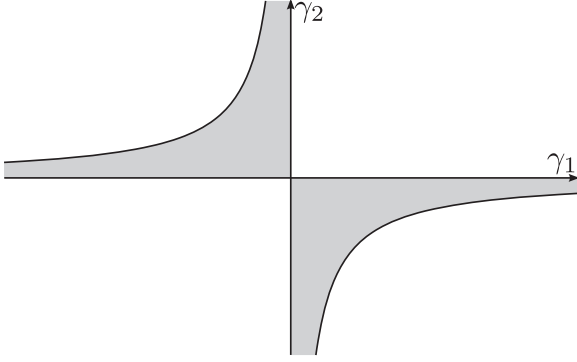
---

*lachlan.smith@northwestern.edu

FIG. 1. Parameters (γ_1, γ_2) of the map Λ_1 such that the period 1 point at the origin is elliptic (gray) and hyperbolic (white). The curves $\gamma_1 = 0, \gamma_2 = 0, 4 + \gamma_1\gamma_2 = 0$ separate regions of different stabilities.

mixing compared to the linear map, whereas pseudohyperbolic points improve mixing rates, and we discuss the governing mechanisms for each case.

II. DISCONTINUOUS DEFORMATION ADDED TO A LINEAR MAP

A. A simple linear map

To study the impact of combined smooth and discontinuous deformations on mixing, we consider a simple linear (smooth) two-dimensional (2D) map with discontinuous deformation added. The smooth map is composed of concatenated horizontal and vertical shears, given by

$$\Lambda_1(x, y) = S_v S_h \begin{bmatrix} x \\ y \end{bmatrix} = A \begin{bmatrix} x \\ y \end{bmatrix}, \tag{1}$$

where

$$S_v = \begin{bmatrix} 1 & 0 \\ \gamma_2 & 1 \end{bmatrix}, \quad S_h = \begin{bmatrix} 1 & \gamma_1 \\ 0 & 1 \end{bmatrix} \tag{2}$$

are horizontal and vertical shear matrices and

$$A = \begin{bmatrix} 1 & \gamma_1 \\ \gamma_2 & 1 + \gamma_1\gamma_2 \end{bmatrix} \tag{3}$$

is their product. This map has a period 1 point at the origin $(\Lambda_1(\mathbf{0}) = \mathbf{0})$, with stability dependent on the eigenvalues of A, given by

$$\lambda_{1,2} = \tfrac{1}{2}[2 + \gamma_1\gamma_2 \pm \sqrt{\gamma_1\gamma_2(4 + \gamma_1\gamma_2)}]. \tag{4}$$

These form a complex conjugate pair, $\lambda_{1,2} = \exp(\pm i\theta)$, when $\gamma_1\gamma_2 < 0$ and $4 + \gamma_1\gamma_2 > 0$, i.e., the gray regions of Fig. 1. In these cases the period-1 point is elliptic, with particle orbits oscillating around the origin as demonstrated in Fig. 2(a), with angle of rotation

$$\cos(\theta) = \tfrac{1}{2}(2 + \gamma_1\gamma_2). \tag{5}$$

Outside of the gray region the real eigenvalues $\lambda_1 = 1/\lambda_2$ correspond to a hyperbolic periodic point, with contraction in the direction of the eigenvector corresponding to $\lambda_i < 1$ and expansion in the direction of the other eigenvector, as demonstrated in Fig. 2(c).

B. The cut-shear-shear map

While linear maps such as Λ_1 are well understood, the addition of discontinuous deformation opens up new possibilities for Lagrangian transport, including pseudoperiodic points. We defined the modified map Λ_2 as that composed of a cut-and-slip deformation followed by the shears that define the map
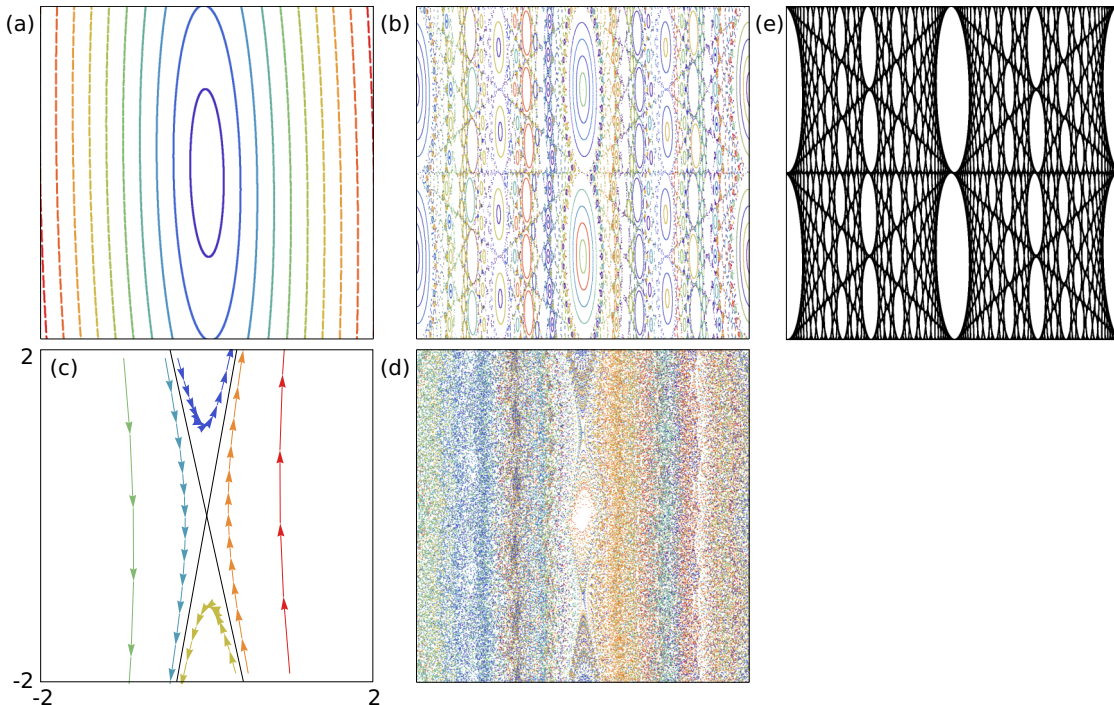

FIG. 2. Orbits of sets of differently colored particles under (a, c) the linear map Λ_1 and (b, d) the discontinuous map Λ_2. In all cases $\gamma_1 = -a = 0.04$. (a, b) $\gamma_2 = -1$. (c, d) $\gamma_2 = 1$. (e) The web of preimages of the Lagrangian discontinuity for the case in panel (b).

Λ_1 [8], i.e.,

$$\Lambda_2(x,y) = S_v S_h C(x,y), \tag{6}$$

where

$$C(x,y) = [x + a\,\mathrm{sgn}(y), y] \tag{7}$$

and periodic boundary conditions are imposed at $y = \pm 2a/\gamma_1$. Explicitly, the map Λ_2 is given by

$$
\begin{aligned}
\Lambda_2(x,y) &= (x',y'), \\
x' &= x + \gamma_1 y + a\,\mathrm{sgn}(y), \\
y' &= \left(\gamma_2 x' + y + \frac{2}{|\gamma_1'|}\ \mathrm{mod}\ \frac{4}{|\gamma_1'|}\right) - \frac{2}{|\gamma_1'|},
\end{aligned} \tag{8}
$$

where $\gamma_i' = \gamma_i/a$ are the relative magnitudes of the shear-and-cut deformations. Both the cutting map C and periodic boundaries produce discontinuous deformations that significantly alter the organization of particle transport, as evidenced by the stark contrast between Figs. 2(a) and 2(c) and Figs. 2(b) and 2(d). This map was used to approximate and elucidate the phenomena observed in a model fluid flow [8], where it was found that discontinuous deformations can be produced by fluid flows even when the base flow is Hamiltonian.

For the map Λ_2 the dynamics in the regions $\gamma_1 > 0$ and $\gamma_1 < 0$ are the same (with γ_2 replaced by $-\gamma_2$); therefore, we only consider the dynamics in the region $\gamma_1 > 0$. Also, it has been shown that the map Λ_2 only has period-1 points when $a < 0$ [8], as this results in a balancing between the horizontal shear and cutting deformations at the points $[4na/(\gamma_1\gamma_2), \pm a/\gamma_1]$ for $n \in \mathbb{Z}$. The dynamics for $a > 0$ are considered briefly in Ref. [8]; however, we do not consider this case here because we are interested in the interplay between classical periodic points and pseudoperiodic points. While the horizontal width of the domain is infinite, the Lagrangian coherent structures repeat themselves with horizontal period $4/|\gamma_1'\gamma_2|$. Therefore, keeping $|\gamma_1'| = 1$ ($\gamma_1 = -a$) and $|\gamma_2| = 1$ fixed, the periodic height and periodic width are both equal to 4, and the square domain $[-2,2) \times [-2,2)$ completely characterizes the transport and mixing properties of the map. Changing $|\gamma_1'|$ and $|\gamma_2|$ only serves to change the vertical and horizontal scales of the domain, and does not affect the gross arrangement of particle motion or mixing characteristics.

Since the smooth deformations that comprise the map Λ_2 are identical to the linear map Λ_1, it follows that material that is not affected by the cut or periodic boundary experiences identical motion under both maps. This is represented mathematically by the fact that the Jacobian of Λ_2, i.e., the matrix $(\partial \Lambda_2^i / \partial x_j)$, is equal to A at all points where it is defined. Therefore the period 1 points located at $[4na/(\gamma_1\gamma_2), \pm a/\gamma_1]$, $n \in \mathbb{Z}$, share the same stability properties as the period 1 point at the origin for the linear map Λ_1, elliptic in the gray region of Fig. 1 and hyperbolic in the white region. Having the same Jacobian also means that the Lyapunov exponent is identical for both maps (in regions where it is defined). Therefore, if the discontinuous deformations were ignored, both maps would be expected to have similar mixing characteristics under the classical theory of mixing by smooth deformations.

Consider, however, the impact of the addition of cutting on particle orbits; Fig. 2 shows that there are fundamental differences to the Lagrangian topology when cutting is included. In Fig. 2(a) the parameters of the map Λ_1 are such that the period-1 points are elliptic, and particles orbit around the origin under the linear map. However, when cutting is added in Fig. 2(b), higher periodicity elliptic point chains are created, forming a fractal tiling of nonmixing islands. In this case, the map is conjugate to a piecewise isometry; i.e., after an appropriate change of coordinates the entire fluid deformation field comprises solely solid body rotations, and patterns such as this have been found in many contexts [23,26–32]. Under smooth deformation theory (specifically the Poincaré-Birkhoff theorem) these chains of elliptic periodic points should be interleaved with chains of hyperbolic periodic points. We have shown previously that when the cut map is approximated by a highly localized smooth shear that is the case [8]. However, a discontinuous cut destroys these hyperbolic points, leaving pseudohyperbolic points that play a similar role to their classical hyperbolic counterparts in generating mixing in the ergodic set among the nonmixing islands. The ergodic set is shown in Fig. 2(e) for this case and is found by considering all locations where the discontinuous deformation will eventually occur, which is equivalent to the closure of the set of preimages of the Lagrangian discontinuities, i.e.,

$$D^s = \left\{ D_n^s = \Lambda_2^{-n}(D_1^s), n > 0 \right\}, \tag{9}$$

where D_1^s are the Lagrangian discontinuities given by the curves $y = 0, \pm 2a/\gamma_1$, straight lines for this map but in general codimension 1 structures of arbitrary geometric complexity; see [33] for a three-dimensional (3D) example. Evidence suggests that the closure of the ergodic set, $\overline{D^s}$, for the map Λ_2 is a fat fractal for almost all sets of parameters [27], i.e., the set has positive Lebesgue measure (area) and fractal boundary.

Changing the sign of the vertical shear in the linear map Λ_1, i.e., γ_2 to $+1$, results in hyperbolic period 1 points that create directions of expansion and contraction [Fig. 2(c)]. The same contraction and expansion is experienced by all material under the map Λ_2; however, the cutting creates many more hyperbolic periodic points whose positions and periodicity match those of the elliptic periodic points in Fig. 2(b). As for the case with negative vertical shear, smooth deformation theory predicts elliptic periodic points that interleave each chain of hyperbolic points, and these exist when the cut is approximated as a highly localized shear. However, these are again destroyed by the discontinuous cut, leaving pseudoelliptic points that create leaky regions where particles are trapped for long periods of time [Fig. 2(d)]. However, unlike the nonmixing regions created by elliptic periodic points, particles are able to enter and exit the leaky regions created by pseudoelliptic points.

III. THE IMPACT OF CUTTING ON MIXING RATES

To study the impact of discontinuous deformation on mixing quality and mixing rates, the mix-norm [20] is used to measure the mixing achieved by the maps Λ_1 and Λ_2. The mix-norm provides a measure of how well mixed a scalar field is, and its rate of decay quantifies the rate of mixing.

As opposed to the Lyapunov exponent, the mix-norm is able to quantify the effect of discontinuous deformation. The mix-norm is similar to Danckwert's intensity of segregation [34], except the mixing quality at every length scale is considered simultaneously, rather than at a single fixed length scale. Exponential decay of the mix-norm indicates strong mixing, whereas subexponential decay indicates only weak mixing or ergodicity. In particular, when the map is linear, such as Λ_1, the decay rate of the mix-norm can be predicted as half the magnitude of the Lyapunov exponent [20], i.e.,

$$\Phi(c_N) = \Phi(c_0) \exp\left(-\frac{\sigma}{2}N\right), \tag{10}$$

where $\sigma = \max(\ln|\lambda_{1,2}|)$ is the Lyapunov exponent.

Starting with some initial scalar field $c(x,y)$—representing concentration, heat, etc.—the mix-norm $\Phi(c_N)$ after N iterations of a map Λ is given by

$$d(c_N, \boldsymbol{p}, s) = \frac{1}{\text{vol}[B(\boldsymbol{p},s)]} \int_{\boldsymbol{x} \in B(\boldsymbol{p},s)} c_N(\boldsymbol{x}) d\boldsymbol{x}, \tag{11}$$

$$\phi(c_N, s) = \left[\int_{\boldsymbol{p} \in D} d^2(c_N, \boldsymbol{p}, s) d\boldsymbol{p} \right]^{1/2}, \tag{12}$$

$$\Phi(c_N) = \left[\int_{s=0}^{w} \phi^2(c_N, s) ds \right]^{1/2}, \tag{13}$$

where $d(c_N, \boldsymbol{p}, s)$ is the average of c_N over the ball $B(\boldsymbol{p},s) = \{|\boldsymbol{x} - \boldsymbol{p}| < s/2\}$, $\phi(c_N, s)$ is the L^2-norm of d over all points in the domain D, and $\Phi(c_N)$ is the L^2-norm of ϕ over length scales in the range 0 to the size of the domain w. As the domain used here is the square $[-2,2)^2$, the size $w = 4$. While the numerical method proposed by Mathew *et al.* [20] based on computation of the Fourier power spectrum of the scalar fields c_N is both fast and accurate for smoothly deforming systems, the presence of discontinuous deformations results in discontinuous interfaces within the concentration fields c_N and hence Fourier power spectra are not reliable. Instead, the mix-norm Φ is computed by numerical approximations of the integrals in Eqs. (11)–(13); for full details, see Ref. [33].

The initial scalar field used to test the mixing efficiency of the maps Λ_1, Λ_2 is $c_0(x,y) = \cos(\pi y/2)$ (Fig. 3), which has mix-norm $\Phi(c_0) = 4.0923$.

A. The elliptic case: Mixing enhancement

Considering the cases when the period 1 points are elliptic, i.e., γ_1, γ_2 are in the gray region of Fig. 1 and the eigenvalues are of the form $\lambda_{1,2} = \exp(\pm i\theta)$: The nature of θ/π (rational or irrational) dictates different mixing behavior for the maps Λ_1, Λ_2.

1. Rational rotation

When θ/π is a rational number of the form m/n, every point in the domain becomes periodic under the linear map Λ_1 (with periodicity $2n$), and so no mixing can occur. This is demonstrated for $\theta = \pi/3, \pi/4$ by the return of the scalar fields c_N in the top rows of Figs. 4(a) and 4(b) to the initial scalar field c_0. Therefore, the mix-norm $\Phi(c_N)$ always evolves periodically in these cases, as demonstrated by the open squares and open triangles in Fig. 5, with period 3 evolution for $\theta = \pi/3$ and period 4 evolution for $\theta = \pi/4$ [35].
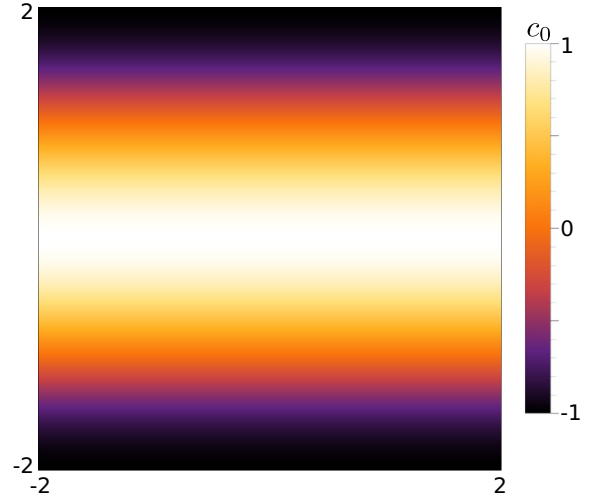

FIG. 3. The initial scalar field $c_0(x,y) = \cos(\pi y/2)$ in the square domain $[-2,2)^2$ that is used to demonstrate the impact of cutting on mixing using the maps Λ_1, Λ_2.

On the other hand, for the map Λ_2 under these conditions the measure-zero ergodic set interleaves a dense tiling of polygons, as demonstrated in thick black in Fig. 6. For $\theta = \pi/3$ the tiling of polygons is simple [Fig. 6(a)], comprised of hexagons and triangles; however, for other rational values of θ/π it is complex and fractal [36]. When $\theta = \pi/3$, particles that are not in the measure-zero chaotic set all have low-period orbits with periodicities that are factors of 12 (period 6 inside the hexagons and period 12 inside the triangles), and the scalar field returns to its initial configuration almost everywhere after 12 iterations (the lowest common multiple of all the periodicities), as shown in the bottom row of Fig. 4(a). While the evolution of the scalar field and hence the mix-norm is periodic under both the linear map Λ_1 and discontinuous map Λ_2 [open and solid squares in Fig. 5], with the cut included (solid squares) the scalar field reaches a lower minimum mix-norm, and hence a more well-mixed state. This temporary mixing enhancement is produced by the creation of discontinuous interfaces within the scalar fields, whose positions coincide with the web of preimages of the Lagrangian discontinuity. When diffusion is included, these discontinuous interfaces create infinite gradients in the scalar field and hence strong diffusion. For 1D interval exchange transformations (IETs) it has been shown that with diffusion included, the discontinuous interfaces created by CS actions can significantly enhance the rate of mixing, even when the underlying CS process is periodic [14]. Similar phenomena will occur when chemical reactions are included, where the discontinuous interfaces provide new sites for reaction.

Considering another relatively simple case with $\theta = \pi/4$, the web of preimages of the Lagrangian discontinuity forms a fractal tiling of octagons [Fig. 6(b)]. Since the periodicity of the octagons scale inversely with their size, there exist arbitrarily small octagons with arbitrarily long periods. Therefore, the range of periodicities is infinite, and a lowest common multiple does not exist. This means that while a large portion of the domain returns to its initial configuration after 16 iterations [bottom row of Fig. 4(b)], the scalar field never fully unmixes.
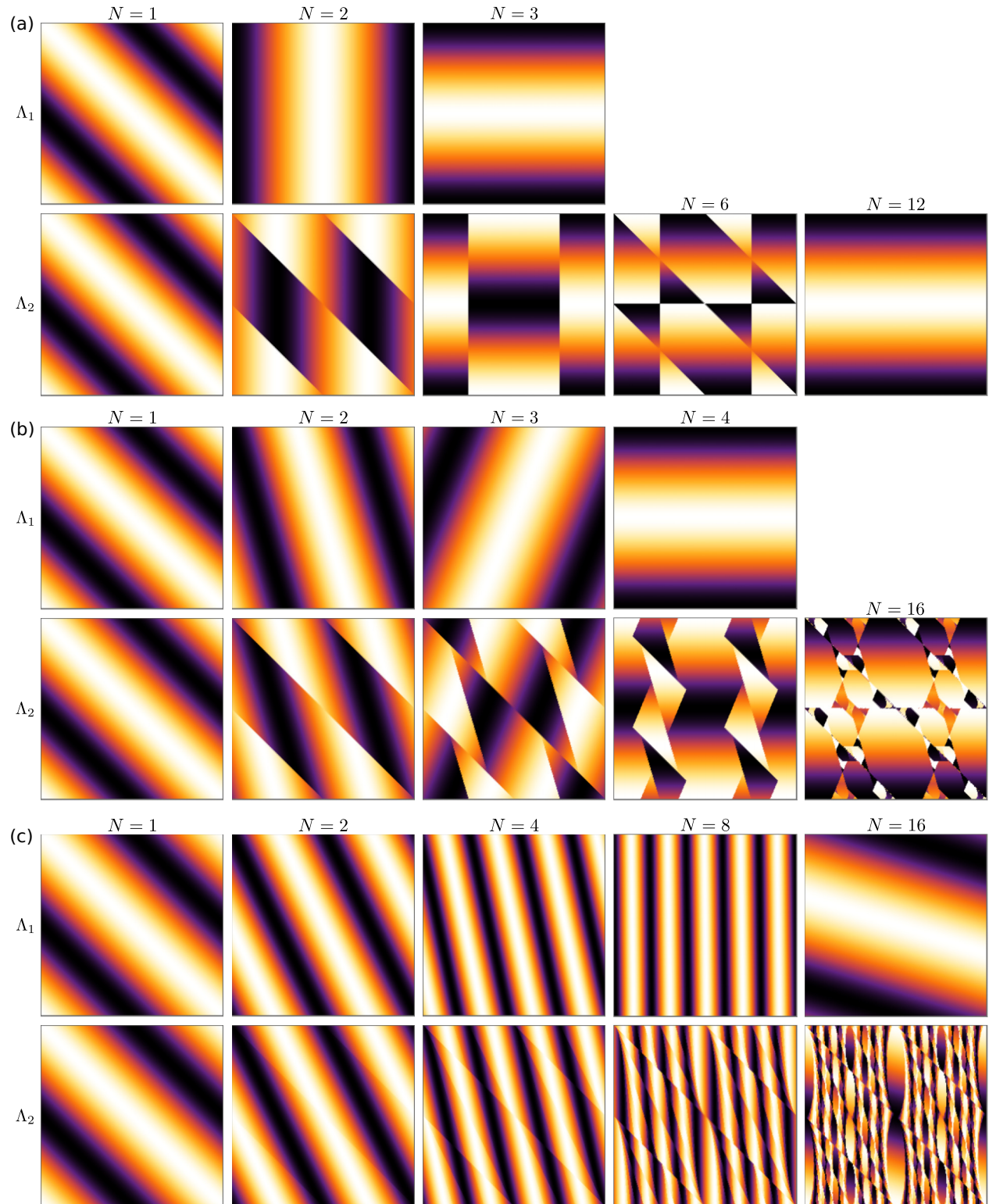
FIG. 4. Iterates of the scalar field c_0 (Fig. 3) under the maps Λ_1, Λ_2. Videos of each sequence can be found in the Supplemental Material [37]. (a) $(\gamma_1, \gamma_2, a) = (1, -1, -1)$ corresponding to $\theta = \pi/3$. (b) $(\gamma_1, \gamma_2, a) = (2 - \sqrt{2}, -1, \sqrt{2} - 2)$ corresponding to $\theta = \pi/4$. (c) $(\gamma_1, \gamma_2, a) = (0.04, -1, -0.04)$ corresponding to $\theta/\pi \approx 0.0638$.

The cases $\theta = \pi/3, \pi/4$ are the simplest examples of a rational rotation angle, and for other values of m and n the tiling of polygons is more complex and always fractal [36]. This means that polygons with arbitrarily long periods can always be found, and hence a lowest common multiple of periods never exists. Therefore, the scalar field will never fully unmix, like the $\theta = \pi/4$ case.
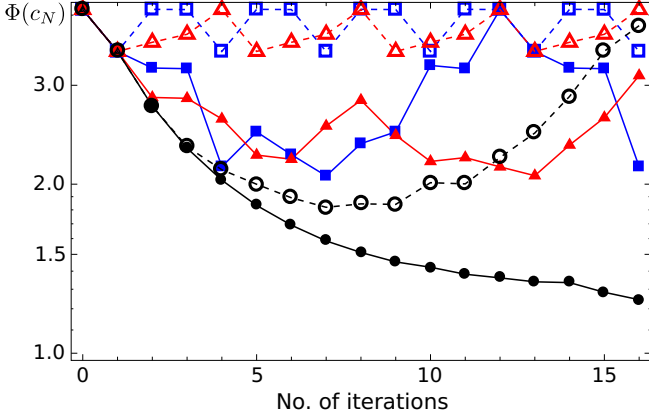
FIG. 5. Log-linear plot of the evolution of the mix-norm of the initial scalar field c_0 (Fig. 3) under the maps Λ_1 (open symbols connected by dashed lines) and Λ_2 (closed symbols connected by solid lines). Blue squares: $(\gamma_1,\gamma_2,a) = (1,-1,-1)$ corresponding to Fig. 4(a). Red triangles: $(\gamma_1,\gamma_2,a) = (2-\sqrt{2},-1,\sqrt{2}-2)$ corresponding to Fig. 4(b). Black circles: $(\gamma_1,\gamma_2,a) = (0.04,-1,-0.04)$ corresponding to Fig. 4(c).

2. Irrational rotation

Conversely, when θ/π is irrational, each point in the domain is quasiperiodic under the linear map Λ_1 and particle orbits densely fill an ellipse. In this case there is still no net mixing and the mix-norm evolves quasiperiodically, as demonstrated by the open circles in Fig. 5 that correspond to the scalar fields in the top row of Fig. 4(c). In this example the scalar fields c_N never exactly return to their initial configuration c_0, though there is qualitative similarity after 16 iterations.

When cutting is introduced, the tiling of polygons formed by the web of preimages of the Lagrangian discontinuity in the rational case becomes a tiling of ellipses in the irrational case, whose complement forms a fat fractal, as demonstrated in Fig. 6(c) for $(\gamma_1,\gamma_2,a) = (0.04,-1,-0.04)$, corresponding to an irrational rotation angle $\theta/\pi \approx 0.0638$. For such irrational cases, none of the orbit periodicities within the nonmixing islands are rational, so the scalar fields c_N can never return to their initial state [bottom row of Fig. 4(c)]. While the mix-norm decreases monotonically for the first 16 iterations [closed circles in Fig. 5], this will not continue indefinitely. Eventually many of the ellipses will reorient (approximately) to their initial configuration, yielding a mix-norm close to the initial value.

In general, when the period 1 points are elliptic the addition of discontinuous cutting deformations enhances mixing compared to the linear map, although the map may still be periodic almost everywhere, resulting in periodic cycles of mixing and unmixing. This enhancement is achieved by the creation of discontinuous interfaces within the scalar field that coincide with the web of preimages of the Lagrangian discontinuity. When additional physics such as diffusion and reaction are included, these discontinuous interfaces create infinite concentration gradients that promote diffusion and reaction.

B. The hyperbolic case: Mixing impediment

In contrast to the elliptic case, when the period 1 points are hyperbolic (the white region in Fig. 1) mixing is impeded
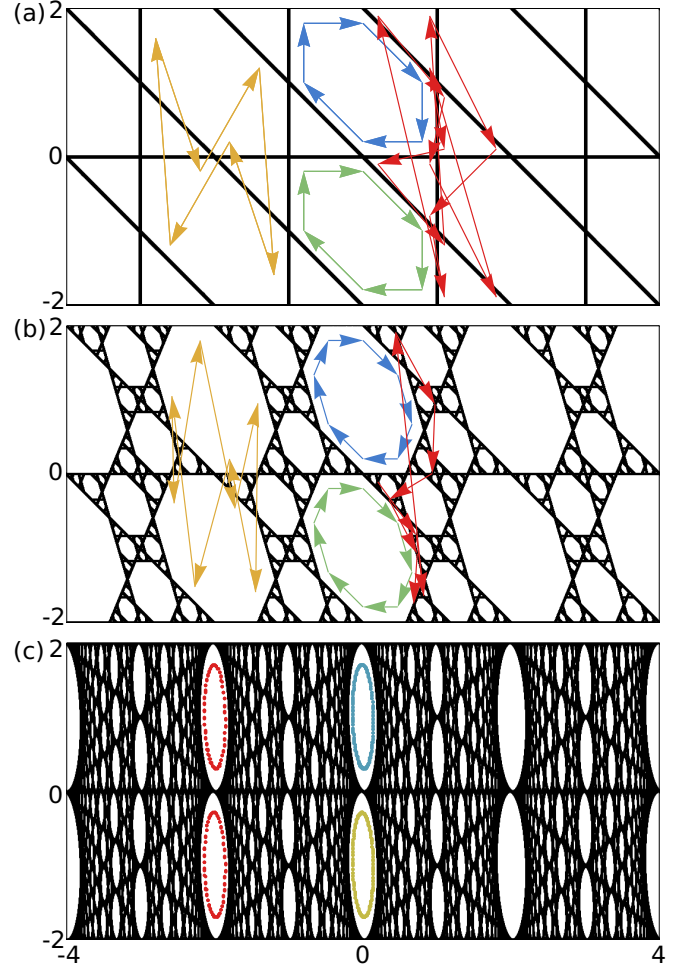

FIG. 6. Particle orbits (colored arrows or points) and web of preimages of the Lagrangian discontinuities (thick black) for (a) $\theta = \pi/3$, (b) $\theta = \pi/4$, and (c) θ/π irrational corresponding to $(\gamma_1,\gamma_2) = (0.04,-1)$. (a) The blue, green, and brown orbits are period 6, and the red orbit is period 12. (b) The blue, green, and brown orbits are period 8, and the red orbit is period 1944, though only the first nine iterates are shown. (c) The blue, brown, and red orbits all have infinite period and fill an ellipse (blue, brown) or a pair of ellipses (red).

when cutting is added. Under the linear map the bands in the concentration fields c_N align along the unstable manifold of the hyperbolic period 1 point and decrease in width by a factor of $\max(\lambda_{1,2})$ after each iteration [demonstrated in the top rows of Figs. 7(a) and 7(b)]. This results in exponential decay of the mix-norm, as shown by the linear trends for the open symbols in Fig. 8. Moreover, the mix-norm decays at the rate predicted by the Lyapunov exponent according to Eq. (10), shown as the dashed lines in Fig. 8. Note that the initially faster decay than predicted is caused by the initial reorientation of the bands in the scalar fields c_N along the unstable manifold of the hyperbolic period 1 point (Fig. 7).

In contrast, when cutting is introduced there are obvious light and dark regions in the scalar fields c_N that indicate a lack of mixing, and these are not present for the linear map (Fig. 7). These regions are created by the pseudoelliptic points that interleave the chains of hyperbolic points, loosely
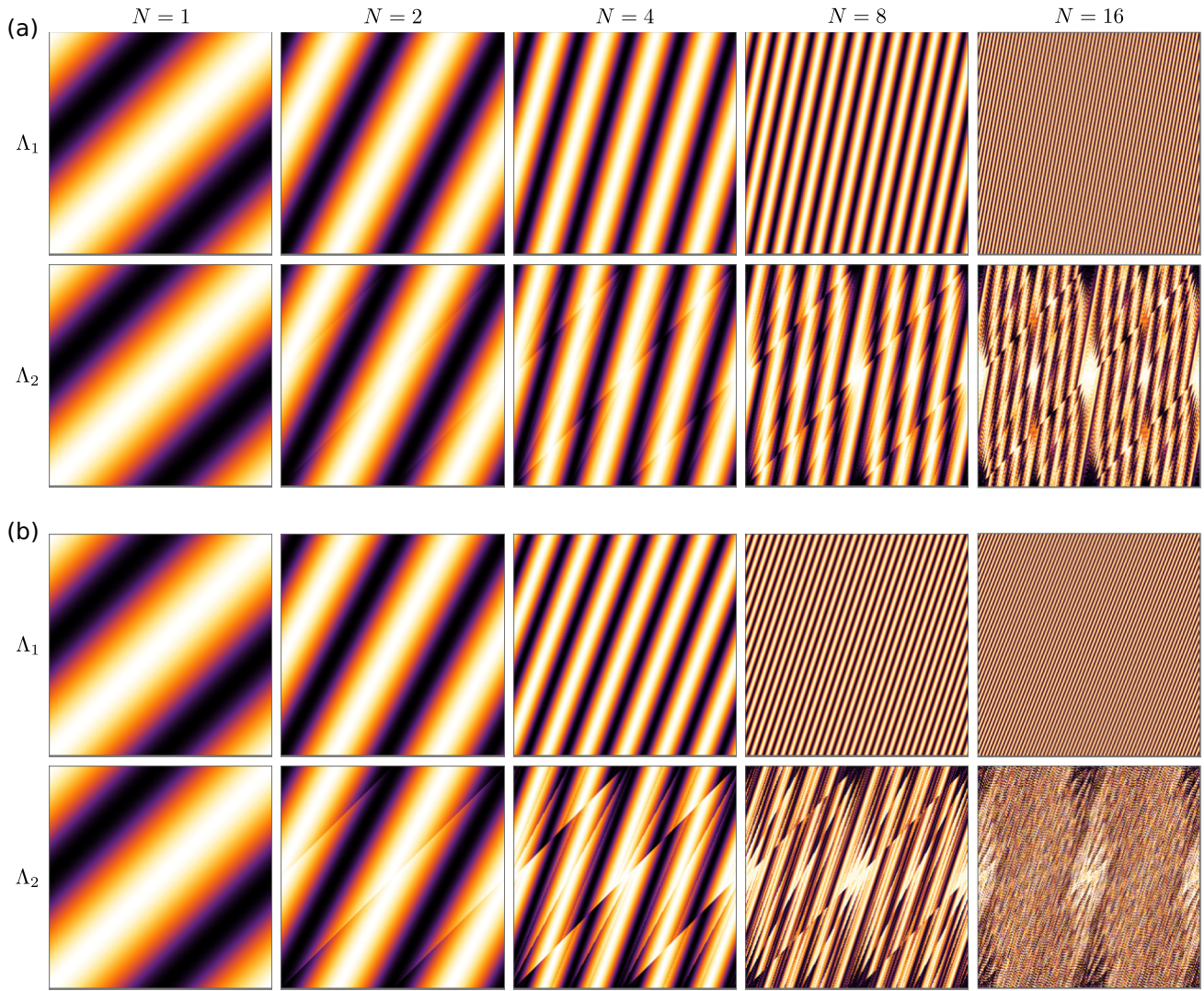
FIG. 7. Iterates of the scalar field c_0 (Fig. 3) under the maps Λ_1 and Λ_2. Videos of each sequence can be found in the Supplemental Material [37]. (a) $(\gamma_1, \gamma_2, a) = (0.04, 1, -0.04)$. (b) $(\gamma_1, \gamma_2, a) = (0.16, 1, -0.16)$.
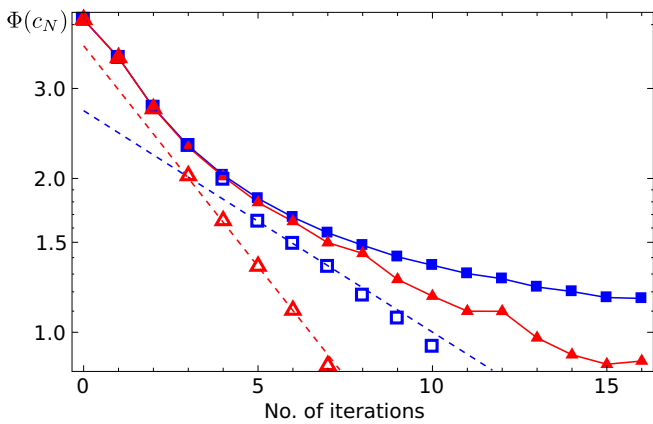

FIG. 8. Log-linear plot of the evolution of the mix-norm of the initial scalar field c_0 (Fig. 3) under the maps Λ_1 (open symbols) and Λ_2 (closed symbols). Blue squares: $(\gamma_1, \gamma_2, a) = (0.04, 1, -0.04)$. Red triangles: $(\gamma_1, \gamma_2, a) = (0.16, 1, -0.16)$. In each case the decay rate predicted by Eq. (10) is shown dashed.

confining particles in a leaky region. In both cases considered, this results in a reduced rate of mixing compared to the linear map, shown by the subexponential decay of the mix-norm (the closed symbols in Fig. 8). Therefore, the addition of cutting results in a shift from strong mixing to weak mixing on the ergodic hierarchy, even though the underlying smooth deformation, and hence Lyapunov exponent, is the same for both maps.

Comparing the two cases shown in Figs. 7 and 8, the case with larger magnitude horizontal shear and cut, $\gamma_1 = -a = 0.16$ [Fig. 7(b) and triangles in Fig. 8], results in better and more rapid mixing for both the linear map Λ_1 and the discontinuous map Λ_2. For the linear map Λ_1, this is predicted by the higher Lyapunov exponent according to Eq. (10), and indicates that for the discontinuous map Λ_2 the mixing rate is still linked to the Lyapunov exponent, even though the decay rate of the mix-norm cannot be directly predicted by the Lyapunov exponent. This correlation between the relative decay rate of the mix-norm and Lyapunov exponent is expected because regions that are not affected by the

discontinuous deformation experience the same expansion and compression deformation as the linear map Λ_1, creating exponential decrease in the widths of the bands observed in the scalar fields c_N (Fig. 7).

It is not clear whether reduced mixing rates should be expected in general systems that combine smooth deformation with a positive Lyapunov exponent and discontinuous deformations The question is whether hyperbolic and pseudoelliptic points form the complete set of buiding blocks in those cases, like hyperbolic and elliptic points in linear stability analysis. If that is the case, then the decay rate of the mix-norm predicted by the Lyapunov exponent can only be used as a lower bound for the decay rate when discontinuous deformations are present, although the Lyapunov exponent can still be used to predict differences in mixing quality for two systems with similar discontinuous deformations.

IV. CONCLUSIONS

The presence of discontinuous deformation can significantly affect mixing processes. Escaping the paradigm of smooth deformations opens up new possibilities for Lagrangian coherent structures such as pseudoperiodic points that play important roles for mixing. The presence of pseudohyperbolic points among a tiling of elliptic points creates an ergodic set and mixing enhancement in cases where the Lyapunov exponent is zero everywhere it is defined, although in some periodic cases the system periodically mixes and unmixes. Conversely, pseudoelliptic points in hyperbolic flow create leaky regions that loosely trap particles and impede the rate of mixing, reducing the mixing rate from exponential to polynomial.

We have also shown that in systems with discontinuous deformations, such as valved flows, granular flows, and shear-banding materials, traditional measures of mixing, such as the Lyapunov exponent, do not reveal the full picture. These measures only capture the impact of smooth deformations, and other measures, such as the mix-norm, are required to capture the impact of both smooth and discontinuous deformation.

Future work should focus on generalizations of the CSS map to form a complete classification of the new Lagrangian structures that can be produced when discontinuous deformation is added to linear systems. This would create a set of building blocks to understand the mixing and transport phenomena in systems where discontinuous deformation is added to nonlinear systems, like elliptic and hyperbolic points in the linear stability analysis of conservative dynamical systems. If it can be shown that elliptic, hyperbolic, pseudoelliptic, and pseudohyperbolic points form the complete set of building blocks, then more general statements regarding mixing enhancement and impediment could be made. Furthermore, the CSS map should be extended to three dimensions, where the extra topological freedom opens up yet more possibilities for new transport structures and is more physically relevant. In particular, due to the connection between the CSS map and the 2D reoriented potential mixing (RPM) flow [8], it is expected that a 3D analog of the CSS map will help to understand the mixing phenomena in its 3D analog, the 3D RPM flow [33,38].

Another future direction is to study the effect of combined smooth and discontinuous deformation when additional physics such as diffusion and chemical reaction are considered. Like for IETs [14], it is expected that in the elliptic and pseudohyperbolic cases, the pseudohyperbolic points will create significant mixing enhancement when diffusion is included due to the creation of discontinuous interfaces in the scalar field. This includes cases such as Fig. 4(a), where the discontinuous map is periodic almost everywhere. In the hyperbolic and pseudoelliptic cases, the inclusion of diffusion should enhance mixing, but it will likely still be impeded when compared to the linear map Λ_1.

ACKNOWLEDGMENTS

[1] N.-T. Nguyen and Z. Wu, J. Micromech. Microeng. **15**, R1 (2005).

[2] C. López, Z. Neufeld, E. Hernández-García, and P. H. Haynes, Phys. Chem. Earth Pt. B **26**, 313 (2001).

[3] M. Sandulescu, C. López, E. Hernández-García, and U. Feudel, Ecological Complexity **5**, 228 (2008).

[4] D. C. Mays and R. M. Neupauer, Water Resour. Res. **48**, W07501 (2012).

[5] H. Aref, J. Fluid Mech. **143**, 1 (1984).

[6] J. M. Ottino, *The Kinematics of Mixing: Stretching, Chaos, and Transport* (Cambridge University Press, Cambridge, UK, 1989).

[7] S. W. Jones and H. Aref, Phys. Fluids **31**, 469 (1988).

[8] L. D. Smith, M. Rudman, D. R. Lester, and G. Metcalfe, Chaos **26**, 023113 (2016).

[9] G. Metcalfe and M. Shattuck, Phys. A (Amsterdam, Neth.) **233**, 709 (1996).

[10] I. C. Christov, J. M. Ottino, and R. M. Lueptow, Phys. Rev. E **81**, 046307 (2010).

[11] I. C. Christov, R. M. Lueptow, and J. M. Ottino, Am. J. Phys. **79**, 359 (2011).

[12] G. Juarez, R. M. Lueptow, J. M. Ottino, R. Sturman, and S. Wiggins, EPL **91**, 20003 (2010).

[13] J. M. Ottino and D. V. Khakhar, Annu. Rev. Fluid Mech. **32**, 55 (2000).

[14] R. Sturman, Adv. Appl. Mech. **45**, 51 (2012).

[15] D. V. Louzguine-Luzgin, L. V. Louzguina-Luzgina, and A. Y. Churyumov, Metals **3**, 1 (2012).

[16] P. D. Olmsted, Rheol. Acta **47**, 283 (2008).

[17] J. Boujlel, F. Pigeonneau, E. Gouillart, and P. Jop, Phys. Rev. Fluids **1**, 031301 (2016).

[18] M. Keane, Math. Z. **141**, 25 (1975).

[19] M. K. Krotter, I. C. Christov, J. M. Ottino, and R. M. Lueptow, Int. J. Bifurcat. Chaos **22**, 1230041 (2012).

[20] G. Mathew, I. Mezić, and L. Petzold, Phys. D (Amsterdam, Neth.) **211**, 23 (2005).

[21] M. Keane, Isr. J. Math. **26**, 188 (1977).

[22] A. Katok, Isr. J. Math. **35**, 301 (1980).

[23] A. Goetz, *Piecewise Isometries: An Emerging Area of Dynamical Systems* (Birkhäuser, Basel, 2003).

[24] M. Viana, Revista Matemática Complutense **19**, 7 (2006).

[25] A. Ávila and G. Forni, Ann. Math. **165**, 637 (2007).

[26] P. P. Park, P. B. Umbanhowar, J. M. Ottino, and R. M. Lueptow, Chaos **26**, 073115 (2016).

[27] P. Ashwin, Phys. Lett. A **232**, 409 (1997).

[28] A. Scott, C. Holmes, and G. Milburn, Phys. D (Amsterdam, Neth.) **155**, 34 (2001).

[29] A. Scott, Phys. D (Amsterdam, Neth.) **181**, 45 (2003).

[30] P. Ashwin and A. Goetz, SIAM J. Appl. Dyn. Syst. **4**, 437 (2005).

[31] X.-C. Fu and J. Duan, Phys. D (Amsterdam, Neth.) **237**, 3369 (2008).

[32] G. Hughes, arXiv:1206.5223.

[33] L. D. Smith, Ph.D. thesis, Monash University, Clayton, Victoria, Australia, 2016.

[34] P. V. Danckwerts, Appl. Sci. Res. Sec. A **3**, 279 (1952).

[35] Note that for the scalar field c_0 only n iterations are required and not $2n$, as c_0 has rotational symmetry (through a rotation of π). For more general initial scalar fields, $2n$ iterations are required to return to the initial configuration.

[36] G. Hughes, arXiv:1311.6763.

[37] See Supplemental Material at http://link.aps.org/supplemental/10.1103/PhysRevE.95.022213 for each full video sequence.

[38] L. D. Smith, M. Rudman, D. R. Lester, and G. Metcalfe, Chaos **26**, 053106 (2016).